TRABAJO DE FIN DE MASTER

Characterization of doped GaInP nanowires for photovoltaics.

Caracterización de nanohilos the GaInP con distintos dopados para aplicaciones en Energía Fotovoltaica.

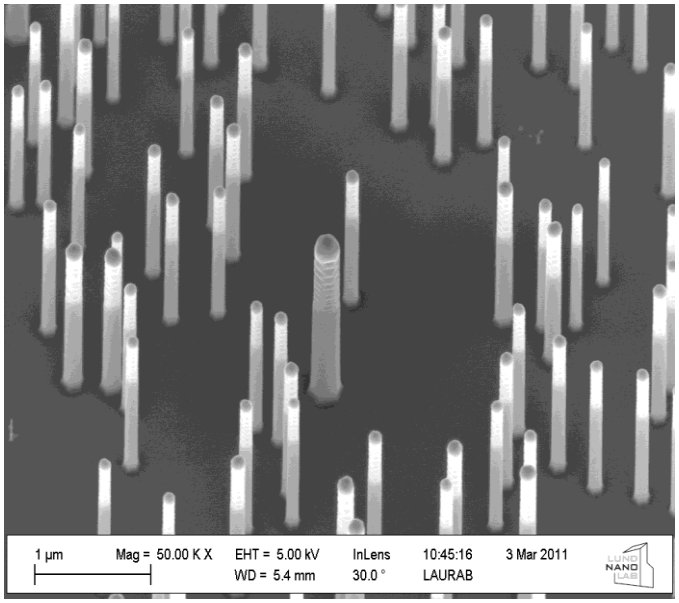

Laura Barrutia Poncela

Directores:

Magnus T. Borgström (magnus.borgstrom@ftf.lth.se)

Jesper Wallentin (jesper.wallentin@ftf.lth.se)

Pedro Hidalgo Alcalde (phidalgo@fis.ucm.es)

Palabras clave: semiconductors nanowires, photoluminescence, electroluminescence, photocurrent, field effect transistor, p-n junction, doping, multijunction devices.

Nanohilos semiconductores, fotoluminiscencia, electroluminiscencia, fotocorriente, transistor de efecto campo, unión p-n, dopado, dispositivos multi-unión.

CONTENTS

ABSTRACT

The interest in renewable energy sources has increased recently, which has resulted in increasing research in solar energy as an environmentally friendly way to obtain electricity. Direct harvesting of solar energy to electricity is called photovoltaics, where III-V semiconductors nanowires can be used to fabricate multijunction solar cells with promise to deliver high efficiency at low cost.

The division of Solid State Physics at Lund University has been working during the last few years on a project for the fabrication of a tandem p-n junction solar cell. In this thesis project, doped nanowires of GaInP have been investigated and evaluated with optical and electrical measurements, with the aim to create high-bandgap p-n junctions. Electrical measurements show that both p- and n-doping can be achieved. Nanowires with p-i-n doping show excellent rectification with reasonably low ideality factors, and generate a clear photocurrent under illumination. Under forward bias, the p-i-n devices give yellow electroluminescence in agreement with photoluminescence experiments.

El interés en las energias renovables ha crecido recientemente resultando en una gran motivación por la energía solar, la cual no causa gran impacto medioambiental a la hora de obtener electricidad. En relación con la energía fotovoltaica, nanohilos de materiales semiconductores del grupo III-V pueden ser usados para fabricar multiuniones de células solares prometiendo una mayor eficiencia y un bajo coste.

El departamento de Física del Estado Sólido de la Universidad de Lund ha estado trabajando durante los últimos años en el projecto AMON-RA con el fin de obtener una nueva tecnología basada en la obtención de una célula solar tipo tándem con el uso de nanohilos semiconductores del grupo III-V. En este projecto de Máster, uniones p-n de nanohilos de GaInP dopados han sido investigados y caracterizados con medidas ópticas y eléctricas con el fin de obtener un alto gap de energía prohibida necesario en este projecto AMON-RA mencionado anteriormente.Contactos p y n han sido capaz de ser fabricados y estudiados. Uniones p-i-n han sido caracterizadas obteniendo una excelente curva de rectificación y fotocorriente al iluminar el dispositivo, con un razonable factor de idealidad. Por otro lado, la aplicación de voltage en el dispositivo ha dado lugar a la emisión de luz en el rango amarillo, resultado que concuerda con las medidas de fotoluminiscencia obtenidas.

1. INTRODUCTION

The demand for electricity has been steadily increasing for many years. Some of the methods of generating electricity by use of for instance as fossil fuels, create major environmental problems and will eventually be depleted. One of the most promising renewable energy sources is solar energy which is plentiful and does not have major contamination problems.

In photovoltaics, the solar photon flux is converted into electricity. The traditional material which dominates the market of these solar cells is silicon because of its low cost. However, silicon is limited in performance with an efficiency around 14 % -19% **[1],** mainly due to its single bandgap.

The spectrum of solar light is spread across the visible and near infrared ranges with a small part in the near ultraviolet. Photons with energy lower than the band gap are not absorbed. High-energy photons are absorbed and contribute to the photocurrent, but since the carriers thermalize to the band edge all excess energy is lost as heat.

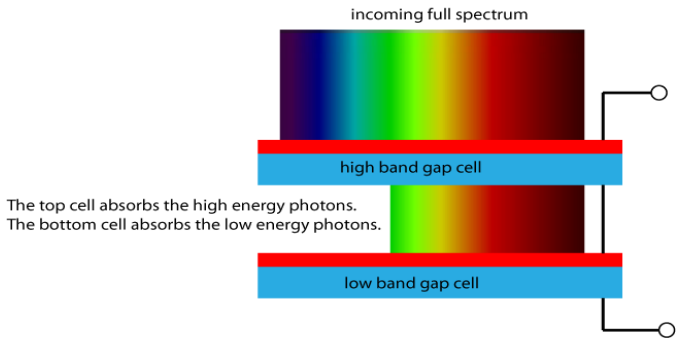

Figure 1: Figure of the solar spectrum absorbed by tandem solar cells. Adapted from ref. **[2]**

Over the years, there has been a lot of research work towards increasing the efficiency of solar cells. The efficiency is much improved with the use of multi-junction solar cells, shown

in Fig.1. Photons that hit the top cell with energy hv lower than the top band gap segment, will be transmitted to the bottom of the cell and will be absorbed by the low band gap segment if $hv > E_G$. A low-energy segment can be used to absorb the low-energy photons, while a high-energy segment can better utilize the high-energy photons.

Higher efficiency can thus be obtained by using advanced multi junction techniques in III-V semiconductors, around twice the efficiency of silicon cells, but this also leads to much higher costs **[3]**. For this planar bulk technology there is an important parameter in reference to the layer growth, the lattice matching, which requires similar inter atomic spaces between two different materials grown together. In practice, this only allows for certain combinations of materials. More severely, it limits the possible substrate materials to a small and quite expensive set (Ge and GaAs).

In nanowires (NWs), strain due to lattice mismatch is a much smaller problem since the strain can be accomodated in the axial direction **[4].** This allows for a much larger freedom in combining materials, as well as epitaxy on large and cheap silicon substrates.

It is known that semiconductors are important in nanodevices like solar cells, light emitting diodes (LEDs), and for visible and infrared detectors. One of the most important parameters of a semiconductor that determines the use in these technologies is the band gap. In this case, to make the solar cells more efficient, it is necessary to increase the range of the band gaps of the materials to cover a wider spectral range being absorbed. By adjusting the relative proportion of the materials in a ternary alloy, it is possible to tune the band gap.

Nowadays a huge range of alloys can be grown by different growth processes such as Metal Organic Vapor Phase (MOVPE) technique providing a high control during growth process. Different complex NWs structures are able to grow epitaxially in dense NW array directly on silicon wafers.

The EU project AMON-RA (Architectures, Materials, One-dimensional Nanowires for Photovoltaics -Research and Applications) is studying III-V semiconducting NWs for use as solar cells. The main purpose of this project is to find a new technology with potentially higher solar cell efficiency by using SC NWs and inexpensive silicon substrates.

In Figure 2 the target design of the AMON-RA project is shown. NWs are fabricated like multi junction heterostructures (containing several p-n junctions) connected in parallel and integrated in a Si substrate, working as a tandem junction device.

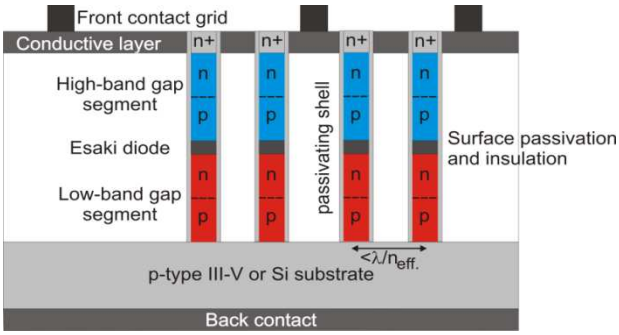

Figure 2: Tandem solar cell scheme proposed by the AMON-RA project. Adapted from ref. [4]

These multijunction heterostructures consist of high band NWs connected in series to low band gap NWs via Esaki diodes providing low resistance through the device, high electrical transmissivity and a high peak tunnel current density **[5]**.

Different materials exhibit different efficiencies and have different cost, thus suitable materials must be chosen for each p-n junction segment. Several projects has been done on the bottom cell by working with InP NWs and it is in a continuing development, which will improve their use in the low band gap segment region with an energy band gap around 1.3eV (at room temperature)[**6**]. In this project we have been focused on the top segment of this tandem p-n junction solar cell, where one of the most promising materials is GaInP. **[7]**

GaInP is a semiconductor composed of indium, gallium and phosphorus which is used in high-power and high-frequency electronics like high electron mobility transistor (HEMT) and heterojunction bipolar transistor (HBT) structures **[8]**. It is used also in LEDs with orange-red, yellow and green colors.

2. THEORY AND BACKGROUND

2.1 Field Effect Transistors (FETs)

GaInP NWs, which are characteristic because of their high band gap, have in this project been studied with optical and electrical measurements to get important parameters (doping, resistance, conductivity, band gap). In order to be able to perform these measurements, Field Effect Transistors (FETs) NWs were built by contacting two metallic electrodes in both sides of the NW which was done by different steps that will be explained later. The idea of this design is to work with the contacts as the drain and source in order to create a MOSFET like device, where the NW defines the conduction channel with a length (*L*), and the two oxide layers (10nm of HfO_2 and 100nm of SiO_2) on Si substrate acting as back gate, as shown in Figure 3:

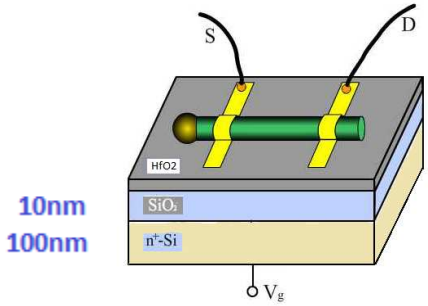

Figure 3: FETs design. Include the NWs 10nm of HfO_2 was deposited on top of 100nm thermally oxidized Si (heavily doped n^+) defines the back gate.

The current-voltage (I_D-V_D) characteristics obtained during the electrical measurements can be modeled like the planar MOSFET structure, with the difference that the geometry of the capacitance is not similar to the planar FETs.

$$I_D = \frac{C_{ox}\mu}{L^2}(V_g - V_{th}) \cdot V_D \qquad (1)$$

L is the length of the conduction channel, V_{th} the threshold voltage (voltage that is needed to be applied to turn on the device), μ is the carrier mobility, and C_{ox} is the capacitance that was calculated for this NW FETs in recent papers **[9]:**

$$C_{ox} = \frac{2\pi\varepsilon_s L}{cosh^{-1}(\frac{r+t_{ox}}{r})} \qquad (2)$$

Here *r* is the radius of the NW and t_{ox} is the thickness of the oxide layer. The electrical permittivity is defined in relation (3).

$$\varepsilon_s = \varepsilon_0 \varepsilon_r \tag{3}$$

$$\varepsilon_r = 3.7 \text{ for } SiO_2;\ \varepsilon_r = 25 \text{ for } HfO_2;\ \varepsilon_0 = 8.85 \cdot 10^{-12}\,\frac{\mathrm{F}}{\mathrm{m}}$$

The doping of the NW can be studied by the back gate measurements. The application of gate bias V_g, introduce free carriers through the device which can be the same type as the original doped carriers or just the opposite. This will be reflected in the conductance that will be increased or decreased depending on the carriers involved. Also by working with the transconductance, the mobility can be extracted.

$$\left.\frac{\partial I_D}{\partial V_g}\right|_{V_{D=const}} = \frac{C_{ox}\mu}{L^2} V_D \tag{4}$$

Using Drude model, once the mobility (μ) is obtained, the carrier concentration (*n)* can be evaluated via equation 5.

$$\sigma = qn\mu \tag{5}$$

Where *q* is the electric charge.

The first part of the project is focused on the study of p and n-type GaInP NWs. Once p and n-type contacts were obtained and characterized to the homogeneously doped NWs, the next step was to work with p-n junctions and tunnel diodes which are the elementary building blocks in solid state photovoltaics.

2.2 Physics of Solar cells

A p-n junction is the most classical structure for solar cells. It is formed when contacting p-type and n-type semiconductors together resulting in a built-in field that will be created due to electrons from the n-side migrating to the p-side. This will create a change of balance in the electric potential at the junction, resulting in a depletion region where the valence band is completely filled and the electrons due to n-doping are removed from the conduction

band. The built in potential can be defined as the difference of electrostatic potential between the conductance band and the valence band.

A plot of the current versus the voltage for a typical p-n junction is shown in Figure 4.

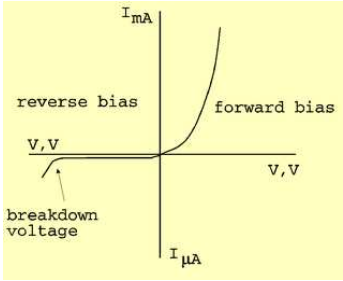

Figure 4: I-V curve for a typical p-n junction. As result of breakdown voltage, this p-n junction seems to be heavily doped. Adapted from ref. [10]

The breakdown voltage observed at reverse bias makes the current increase notably and this can be due to two effects, tunneling effect (which occurs for highly doped samples) and avalanche multiplication (for lowly doped junctions). In tunneling effect, a valence electron from the p type material is able to make a transition to the conduction band on the n side. And in avalanche multiplication (which is less important for solar cells but very important for photodetectors) of electrons, due to the increase of their kinetic energy with the electric field. The breakdown voltage at reverse bias due to the tunneling should be noticeable around a few volts or even more, while for the forward bias it is noticeable around 0.5-2V **[14]**.

The absorption of light (which leads to the creation of electron-hole pairs) and the p-n junction leading to a splitting of those in the depletion region is the fundamental operation of solar cells. These electron hole pairs are the result of the excitation of an electron in the valence band to the conduction band leaving a hole (the absence of an electron).

One important parameter for a p-n junction under illumination is the absorption coefficient α which is the probability of a photon to be absorbed, which is proportional to the probability of the transition from the initial state to the final state and the density of electrons in both states. The absorption depth is related to this coefficient, so α determines how far into a material light of a particular wavelength can penetrate before it is absorbed.

For indirect transitions, this coefficient is also dependent of the available phonons so for indirect band gap materials the absorption coefficient will be smaller. But the absorption depth $1/\alpha$ will be higher **[12].** Gallium Indium Phosphide (GaInP) is characteristic for its direct band gap which involves two particles (the incoming photon and the exited electron) in the absorption process while for indirect band gap materials, like Si and Ge, a third particle (phonon) participates **[11].**

Another important parameter for solar cell efficiency is the recombination which takes part when a semiconductor stops from being in thermal equilibrium because of the injection of carriers due to illumination (like in solar cells) or by applying a voltage. The recombination reduces the current produced by the solar cell. This recombination can be induced by traps, different defects or impurities creating energy levels inside the band gap, or by band-to-band recombination (radiative).

The *I-V* curve of an ideal diode is defined in equation 5 where *I* is the current, I_0 the saturation current, *V* the voltage, *n* the ideality factor and $\frac{kT}{q}$ is the thermal energy which is 0.0258eV at room temperature (300K).

$$I = I_0(\exp\left(\frac{qV}{nkT}\right) - 1) \tag{6}$$

I-V characteristics of a solar cell are obtained by shifting the *I-V* characteristics of a diode in the dark downward by the light generated current.

$$I = I_0\left(\exp\left(\frac{qV}{nkT}\right) - 1\right) - I_L \tag{7}$$

$$I_{0=}eA\left(\sqrt{\frac{D_p}{\tau_p}\frac{{n_i}^2}{N_D}} + \sqrt{\frac{D_n}{\tau_n}\frac{{n_i}^2}{N_A}}\right) \tag{8}$$

I_0 depends on the intrinsic carriers concentration, the cross sectional area *A*, diffusion coefficients $D_{p,n}$; donor and acceptor concentrations $N_{D,A}$; and carrier lifetime $\tau_{p,n}$.If we define the light generated current as being positive, the *I-V* curve of a p-n junction under illumination is shown in figure 5.

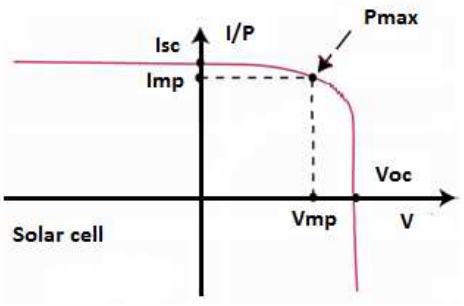

Figure 5: p-n junction under illumination. The maximum value of the current Imp and the voltage Vmp gives the maximum power Pmax. Adapted from ref. [13]

The illumination under light makes the curve to be shifted and working on the first quadrant the power of the device can be obtained.

Relevant parameters involved in the efficiency of solar cells are: short circuit current, open circuit voltage, the filling factor and the efficiency. All of them should be as high as possible. Looking at the Figure5, the short circuit current (I_{sc}) is obtained at zero voltage and is related to the generation and collection of light-generated carriers. I_{sc} gives as an idea about the absorption of the light but the carriers must arrive also at the contacts without recombination. In the case of working with an ideal solar cell, this parameter is equal to the light generated current $I_{sc}=I_L$.

The open circuit voltage V_{oc} can be defined as the maximum voltage available from the solar cell. Working with the equation of the *I-V* curve, the V_{oc} can be defined by equation 9.

$$V_{oc} = \frac{nkT}{q} \ln\left(\frac{I_L}{I_0}\right) \tag{9}$$

While the light-generated current depends on the collection and generation of carriers, the main parameter of the equation that affects V_{oc} is the saturation current I_0, which depends on the intrinsic carriers concentrations n_i and is related to the recombination that takes part in the solar cell. The intrinsic carrier concentration (n_i) depends on the temperature like $n_i \approx T^{3/2}$, it is appreciable how the recombination increases by increasing the temperature, while the band gap of the semiconductor and also the open circuit decreases. Moreover, higher temperature decreases the band gap so more photons with less energy can be absorb resulting in an increase of the short circuit current **[2]**.

An improvement of both I_{sc} and V_{oc} can be achieved by adding an intrinsic segment between the p and the n side segments. By introducing an un-doped segment, the electric field extends over a wider region and the depletion region is elongated improving the collection of the light generated carriers **[15].** In this project, p-i-n NWs of GaInP will be studied.

The fill factor *FF* can be obtained from the I-V curve and is the ratio between the maximum power and the V_{oc} and I_{sc}.

$$FF = \frac{V_{MAX}I_{MAX}}{V_{oc}I_{sc}} \leq 1 \tag{10}$$

The efficiency η is an important parameter in solar cells and can be described as the ratio between the output power and the input power.

$$P_{MAX} = V_{MAX}I_{MAX} = FFV_{oc}I_{sc} \rightarrow \eta = \frac{P_{max}}{P_{input}} \tag{11}$$

As mentioned before, the improvement of this parameter is been investigated by making tandem solar cells covering the wide range of the solar spectrum. **[12]**

The ideality factor *n* measures the junction quality, by studying this factor we can also study the type of recombination that is taking place. The ideality factor can be obtained from the *I-V* curve, from the slope of the semi logarithm plot of the current versus the voltage:

$$\ln(I) = \frac{q}{nkT}V \rightarrow slope = \frac{q}{nkT} \rightarrow (T = 300K) \rightarrow slope = \frac{1}{n\ 0.0258} \tag{12}$$

There is a theory called Sah-Noyce-Shockey which describes the values of *n*, when *n=1* (ideal diode) the diffusion current dominates and the recombination of the minority carriers is done via band to band or via traps in the bulk areas, while *n=2* is dominated by recombination of carriers in the space region. It is also important to mention that this theory does not explain higher values of this parameter **[16]** and **[17]**.

For better understanding of the solar cell, Figure 6 is shown. While the solar cell is illuminated by light, generation of both electron-hole pairs in both sides of the p-n junction takes place (light generates excess minority carriers in both sides). The carriers move across the junction results in a generated driftcurrent.

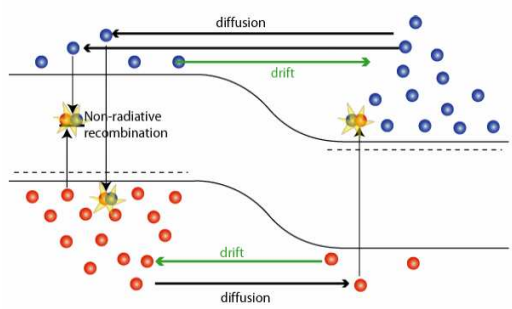

Figure 6: p and n regions showing diffusion and drift carriers of a diode under illumination. Adapted from ref. [12]

The basic requirements to have an efficient solar cell are by obtaining high absorption, high collection probability and low diffusion current. For that, both available carriers must be present, and the collection of these carriers can be done by the electric field present in the p-n junction by spatially separating the electrons and holes. To avoid recombination of these carriers the diffusion current, which is the opposite of the drift current created by the electric field, must be as low as possible **[12].**

2.3 Tunnel diode

Tunnel diode structures were created by Leo Esaki in 1958 who received the Nobel Prize in recognition of his work **[18]**. As mentioned before, they are necessary for contacting the different segments of the Tandem solar cell structure. Tunnel diodes can be defined as heavily doped p^{++}-n^{++} junction.

When the material is heavily doped, the Fermi level lies on the conduction band for the n-type and inside the valence band for the p-type. It is also known that the depletion region *W* is smaller for high doping concentrations, since it follows equation 13. Here N_d is the doping concentration.

$$W \propto \frac{1}{\sqrt{N_D}} \tag{13}$$

In order to increase the desired interband tunneling current, a heterostructure with a type-II band alignment can be used to reduce the tunneling barrier, thus, increasing the probability of tunneling **[6]**. Figure 7 shows the behavior of a tunnel diode for different voltages.

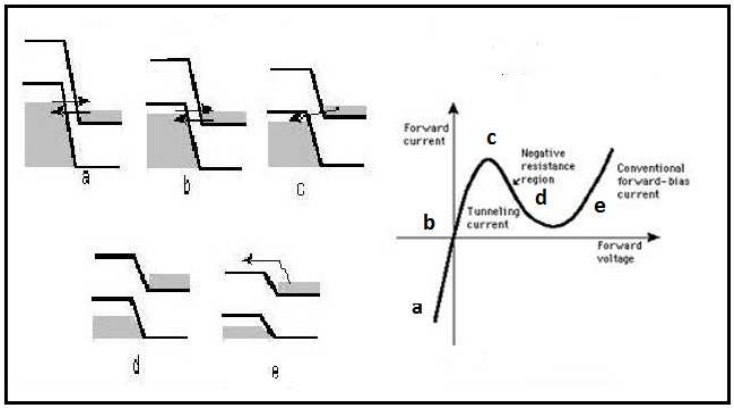

Figure 7: a) I-V curve of a tunnel diode showing the different regions (a-b-c tunneling region, d negative resistance region, e conventional forward current); Adapted from ref. [19]

If the depletion region is thin enough, on the order of 5-20 nm, the electrons will be able to tunnel from the n-doped side to the p-doped side when a bias is applied. When the bias is increased, more and more electrons will be able to tunnel to the p-doped side (a-b regions in Figure 7). At a certain bias it will reach a peak where the Fermi-level on the p-doped side is aligned with the bottom of the conduction band on the n-doped side (c region in Figure 7). The electron states become less aligned with the empty valence band holes states on the p-side resulting in a decrease in current (negative resistance region in Figure 7). If the bias voltage is increased even more, it will start to behave just like an ordinary p-n junction (region e in Figure 7), where the electrons arrive at the p-doped side conduction band, resulting in an exponential increase of current with increasing bias **[14].**

When illuminating a tunneling diode, with a photon energy larger than the band gap, we expect to see a much smaller photocurrent in the tunneling diode compared to the p-n diode, because of the very small depletion region shown before (Fig 10). Note that any photocurrent generated in the tunnel diode is directed opposite of the two p-i-n junctions, and is therefore undesirable.

As mention before, the role of the tunnel diodes in this Tandem Solar Cell is quite important because they act as connections between the different segments providing low resistance through the device. This small resistance signal is proportional to the peak density current. To have a low resistance, the voltage in the tunneling region must be low enough so that energy of electrons which are tunneling is equal to energy states available on the other side

of the barrier. Consequently, current density through the tunnel junction is high (with maximum value of J_P, the peak current density) and the slope from Figure 7 near the origin is therefore sharp. Figure 8 shows the band diagram alignment of the tandem solar cell structure.

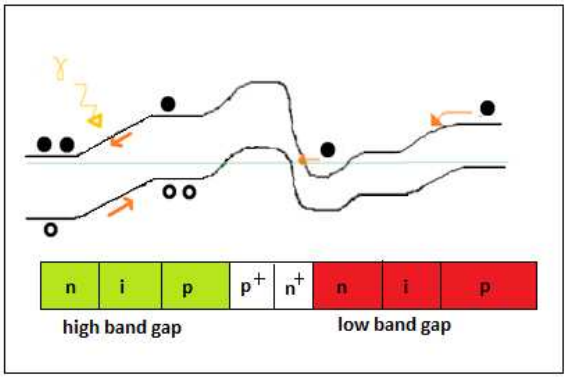

***Figure 8: Sketched band diagram of high band gap p-i-n junction segment connected with a low band gap p-i-n junction segment via Esaki diode. (For clarity,* the change in the Fermi level alignment with respect to the valence band between p and p^{++} regions and n^{++} and n regions has been made unrealistically large).**

2.4 Metal-semiconductor contact

When a metal and a semiconductor are in contact, there is an energy barrier for electron transport from the semiconductor side to the metal side due to the difference in work function between the metal and the SC.

The current-voltage characteristics of a metal-semiconductor contact, is governed by the transport of the charge carriers. According to the *I-V* characteristics, contacts can be divided into two categories, which depends on the Fermi level alignment between both metal and semiconductor interface. A Schottky barrier or rectifying contact can be formed (high contact resistance with respect to the electronic device) but also an Ohmic contact, where linear current-voltage behavior of the device is seen (small contact resistance) **[20]**.

In an ideal semiconductor-metal junction, the work function is represented as ϕ_s, and in the case of a n-type semiconductor, when the work function of the metal $\phi_m > \phi_s$ Schottky contacts will be obtained. For a p-type semiconductor the condition to get Schottky contacts

is the opposite, $\phi_m < \phi_s$**[21].** However this behavior is not always achieved and depends on what materials are connected, and can be chosen as to optimize either Shocttky or Ohmic behavior**.** In real junctions, there is always a high density of states at the interface which will pin the band offset independent of the work functions **[20].** Figure 9 shows surface defects that act as trapping centers with an energy level with in the gap that can influence the *I-V* characteristics.

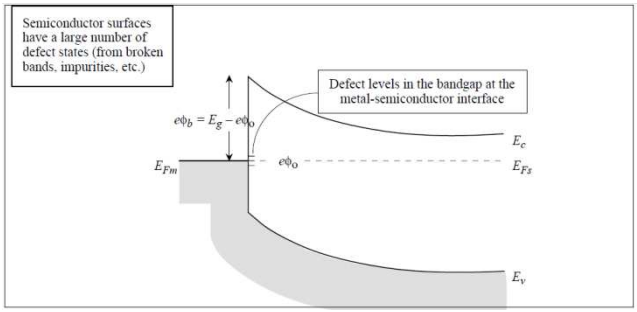

Figure 9: Schottky junction in real systems due to the presence of defects . Here E_{FM} is the Fermi level of the metal, $e\phi_b$ the barrier height, $e\phi_0$ the defect levels, Ec the conduction band, E_{Fs} the Fermi level in the semiconductor and E_v the valence band. Adapted from ref. [21]

One way of making Ohmic contacts is by highly doping the semiconductor resulting in a linear *I-V* curve. As it has been shown before, the depletion region *W* is inversely proportional to the square root of the doping concentration N_d, thus, for higher level of doping, the smaller depletion region is (see Figure 10), and higher probability of tunneling is obtained, providing good contacts with low resistance. In practice, a high doping level is more important than choosing a metal with a suitable work function.

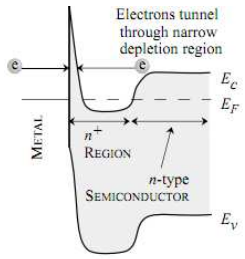

Figure 10: Depletion region of heavily doped SC in contact with a metal. Adapted from ref. [21]

Assuming that enough good contacts can be considered if we have Schottky like contacts with very low barriers, we can describe our band alignment between the semiconductor NW and the two metallic electrodes like Figure 11. ϕ_1, ϕ_2 are the Schottky barriers at the interface which will determine the *I-V* a behavior. E_{Fs} the Fermi level at the source region, E_{FD} Fermi level in the drain region, *Ec* the conduction band and E_v the valence band. The bands will be bended depending on the applied voltage (they will bend upward in the direction of the applied electric field).

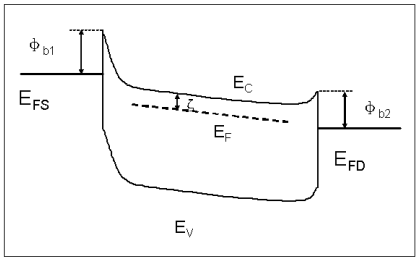

Figure 11: Band diagram showing the bending of the bands of the metal semiconductor interface under bias. Adapted from ref. [22]

The common behavior of *I-V* characteristics in a homogeneously doped semiconductor NW is almost linear, but sometimes a specific case can be achieved, where one of the contacts is good (ohmic and linear) and the other can present a Schottky barrier. A rectifying curve is determined because the electrons aren´t able to go through the NW in one direction due to this barrier which deals to not having an optimized FET.

Making Schottky contacts is not so interesting in this project because low resistance (ohmic) contacts are necessary to link the active regions of the SC devices to the extend circuit. The main requirements of ohmic contacts are that they should have low contact resistance, be thermally stable and have good adhesion and lateral uniformity, surface passivation **[22]**.

3. METHODOLOGY

As has been mention before, Field Effect Transistors (FETs) were done in order to achieve electrical and optical measurements. Different steps were carried on for the contacts design.

3.1 Processing

3.1.1 Growth of the nanowires

The growth of the NWs was done by a group of epitaxy researchers (Jesper Wallentin, Magnus Borgström and Daniel Jacobsson) at the Nanometer Consortium at Lund University.

The Vapor –Liquid-Solid (VLS) method is used for the growth of one-dimensional structures such as NWs. The growth of III-V semiconductor NWs is done by a technique known as Metal-Organic-Vapor-Phase-Epitaxy (MOVPE) where they grow due to a carrier gas containing chemical precursors and gold particles which act as a seed particle. The diameter of the seed particle (in this case Au particle) determines the diameter of the NW (see Figure 12).

Epitaxial growth is also called bottom up fabrication and is illustrated in Figure 12, where the Au particle acts as a catalyst particle staying on top of the structure during the growth.

The growth can be divided in different steps:

1. Deposition of gold particles on the substrate (which is made after pattern design by nanoimprint lithography technique (NIL)).
2. Increase of temperature until the desired temperature is obtained.
3. Source gases are supplied (phosphine (PH_3), trimethylindium (TMIn) and trimethylgallium (TMGa) were used for the growth of GaInP NWs), creating a supersaturation of the III-material in the gold particle, nucleation takes part.
4. NWs start growing at the interface of the gold particle and the substrate (formation of the NW crystals).
5. The seed particle is lifted during the growth NW.

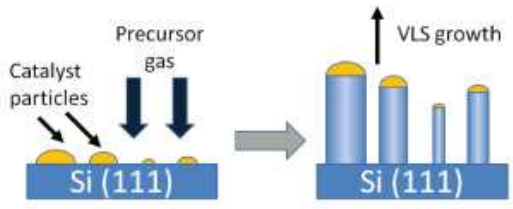

Schematic illustration of the VLS growth process

Figure 12: NWs growth by VLS technique. Au particles deposited on a silicon substrate Si(111). The gold particles together with the precursor gas participate in the growth of the NWs via VLS technique. Adapted from ref. [23]

The growth of the NWs in a specific direction is determined by the crystal symmetry of the substrate. It has been demonstrated that III-V wires usually grow in the [111]B direction **[24]**. Different parameters are controlled during the synthesis of these NWs (length of the diverse regions, diameter, doping) and doping the NWs is one of the most important steps of these devices because by introducing impurity dopants the control of the conductive properties of the NWs can be done. The impurity doping is introduced during growth by supplying special precursors, so-called *in situ* doping. It is also possible to dope NWs *ex situ* with diffusion or ion implantation, but that has not been used in this project.

Hydrogen sulfide (H_2S) was added as a n-type doping precursor and diethyl zinc (DEZn) as p-dopant precursor. One important factor that appears during the growth is tapering, where radial growth on the bottom of the NW segment is seen. Tapering is not desired for for p-n junctions since it could short-circuit the device, but it was controlled with the used of Hydrogen Chloride (HCl) **[25]**.

After the growth of the NWs by the MOVPE technique on a InP(111) substrate, Scanning Electron Microscope (SEM) images were taken in order to get an idea of the distribution of the NWs on the substrate as well as the length, diameter and shapes. The NWs grown have around 80-100nm of diameter and 1.4-1.8µm of length. Looking at the SEM images in Figure 13, the gold particles which were used for the synthesis, can be detected at the top of the NWs. Moreover, the contrast in the wires shows the different regions (p and n-segments).

a) 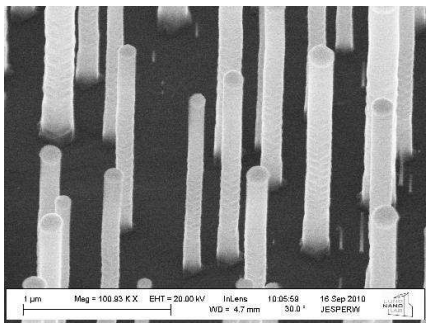

b) 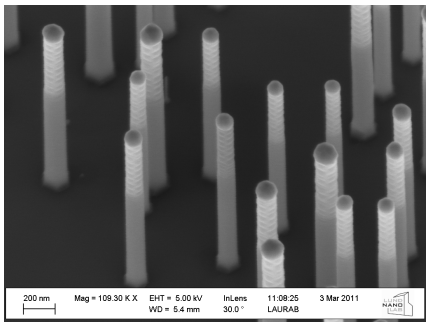

Figure 13: SEM images for a) p-i-n junction and b) tunnel diode

According to previous reports on InP NWs using DEZn as dopant, a periodic twinning in the SEM images can be observed due to the zincblende crystal structure caused by the addition of this precursor for the p-type segment **[4].**

3.1.2 PL Measurements

PL measurements were performed by placing the samples in a cryostat with a temperature around 5-10 K to avoid excitations due to thermal energy. A green laser around 2.3eV is used for the excitation of the sample. The light emitted goes through a monochromator which acts as filter from the signal detected from the laser and also splits the light into the different wavelengths before arriving to the detector (CCD camera) that is connected to the computer that registers the data.

Different samples were studied before being contacted like FETs. The PL measurements were done on single NWs of homogenously p-doped, n-doped and un-doped GaInP, placed on an Au substrate and measured at low temperature (5-10K).

3.1.3 Contacts design

For the processing, the NWs were deposited on a wafer by using clean room paper and carefully touching the substrate where they had grown. Once they were transferred into the different write fields (24 coordinate systems), images were taken by the optical microscope, in dark field mode at high magnitude(x100). The aim of this step is to find a nice NW and determine its length and position in each write field in order to design contacts by lithography, metal evaporation and lift off.

a) 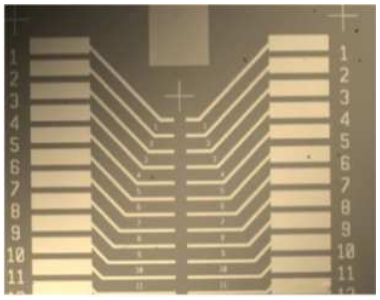 b) 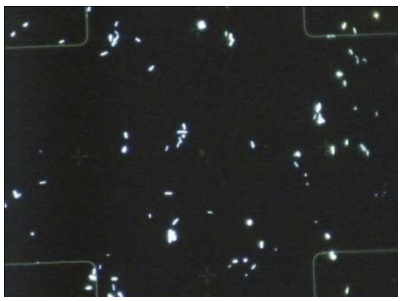

Figure 14: a) $Si/SiO_2/HfO_2$ substrate with24 identical coordinate systems; b) Optical image in dark field mode.

The design of the contacts was done by using Kristian Storm´s program nanodim in Matlab **[26].** Before it, SEM images were taken to recognize both sides of the NWs which can be done by the gold particle which can be distinguished with the use of this microscope. This step was necessary for some samples because the contacts needed to be in some specific regions of the NWs in order to contact the p and n-type regions.

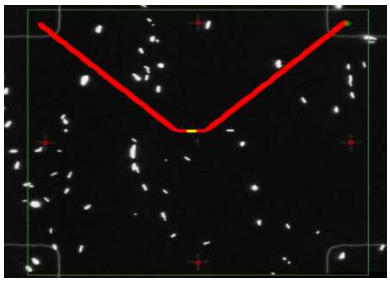

Figure 18: Contacts designed by Kristian Storm´s nanodim in Matlab.

Before Electron Beam Lithography (EBL), the deposition of the resist was done. In this case we used PMMA 950 A6 which is a positive resist and thicker than A5. (A5 and A6 denote the percentage of anisole the PMMA is mixed with) .For a homogeneous deposition of the resist all over the sample a spinner was used.

The exposure of the different samples was carried out with EBL Raith 50. Different parameters like focusing and stigmatism must be taken into account to optimize the exposure.

a) 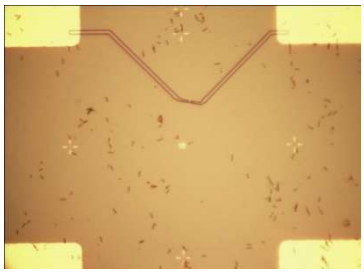 b) 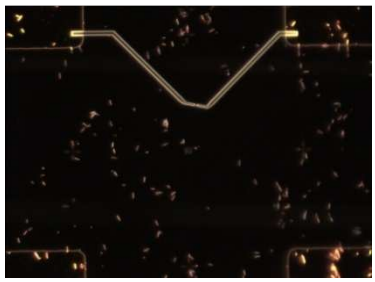

Figure 15: Optical microscope images in bright field (BF) and dark field (DF) mode. a) Sample laurab7 WF15 after EBL exposure BF, b) Sample laurab7 WF15 after EBL exposure (DF).

Development of the resist

After EBL exposure, the resist was developed by using methyl isobutyl ketone/ isopropanol (MIBK for 90s/IPA for 30s). PMMA is a positive resist so the regions which have been exposed will be removed by this development. Figure 15 shows how the sample looks like after this step, both bright field and dark field images were taken.

Ozone cleaner

Ozone cleaner was used before the deposition of the metals to clean the sample from resist residuals from the resist or other kind of contamination.

Etching and passivation

In order to remove oxide layers, n and p-type NWs were etched by using diluted H_3PO_4 :H_2O (1:9) for 2min and H_2SO_4 :H_2O (1:3) for 1min as a recipe, after etching, sulfur passivation was done with NH_4S_x to avoid re-oxidation.

This recipe was changed for some samples, the etching step was changed by working with a diluted HF (1:10) buffer around 1min for some samples and 25s for others. By using HF it etches away the native surface oxides but also serves for passivation, so one step is avoided by changing the recipe.

Deposition of the metals

As has been said before, different factors are involved when deposition of the metal contacts are done. One important parameter is the difference between the work functions from the metal and the semiconductor. There are several studies about contacting semiconductors especially III-V compounds like InP **[6]**. Palladium is one of the common components used in ohmic contacts metallization in III-V SCs.

The deposition of the metals was carried out by working with the Evaporator Avac. For the design of our p-type contacts, palladium has been used as the first component in a multilayer metallization, where its primary function is to serve as an adhesion layer to initiate reactions with the underlying semiconductor.

A Pd/Zn/Pd /Au (10/10/20/70nm) metal combination was used as a recipe to try to obtain ohmic contacts for the p contacts and Ti/Pd/Au (10/10/80nm) was used for n-contacts **[6**] and **[20].** For p-i-n devices, p-type contacts were used for both ends in order to save one EBL step. The use of p-type contacts better than n-contacts was done due to the worst behavior achieved for contacting the p-region.

The decision of trying to obtain a metal thickness around 100nm was because the thickness of the resist (300nm) must be taken into account to avoid problems during the lift-off.

Lift off

In the lift off process the resist is removed by a remover agent, after deposition of the metals, the resist was lifted off with acetone by heating it on a hot plate at 47 ºC for 15min or without heating the acetone and leaving the sample inside it for several hours.

a)  **b)** 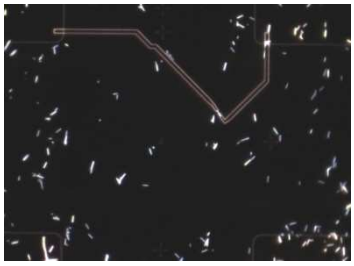

Figure 16: Images taken from an optical microscope in bright field (BF) and dark field (DF) mode. a) Sample laurab6 of WF2 after evaporation (BF); b) Sample laurab6 WF2 after evaporation (DF).

Temperature anneling processing is often used to diffuse the dopants from the contacts into the semiconductor to have a highly doped contact region, but in this case, annealing step was avoided due to no improvement observed on InP NWs previosuly contacted in the same way.

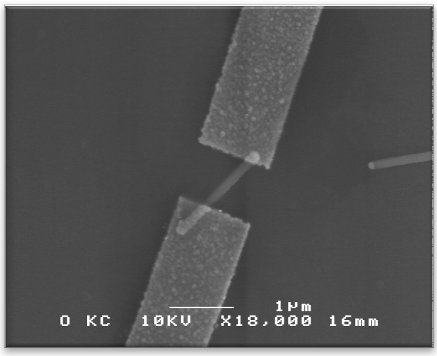

Figure 17: SEM images of one device after contacts design.

Figure 17 shows one device after contact design where metal deposition can be seen in both extremes of the nanowire, also the gold particle can be identified at the top end of the NW.

3.1.4 Electrical measurements

The electrical characterization was done at room temperature using Probe Station Cascade 11000B which is a semiconductor characterization system consisting of a chuck where the sample is held in place by vacuum to make sure it is stuck during the measurements . The measurement setup rests on an anti-vibration platform. Different *I-V* measurements are done connecting two probes between the ends of the selected NW. Also back gate measurements can be performed by contacting the chuck. The data was collected with Keithley 4200 Program in a computer.

In order to perform both photocurrent spectroscopy and electroluminescence measurements, the samples were fixed on a 14 pin bond chip by bonding the EBL pads to different pins with Al wire.

4. RESULTS AND DISCUSSION

4.1 Photoluminescence

Photoluminescence measurements (carried at low temperature 4.2K) were done in order to obtain information about the emission of photons (luminescence) due to excitation of electrons to higher states by absorbing photons and then re-radiating. The time between absorption and emission is around nanoseconds.

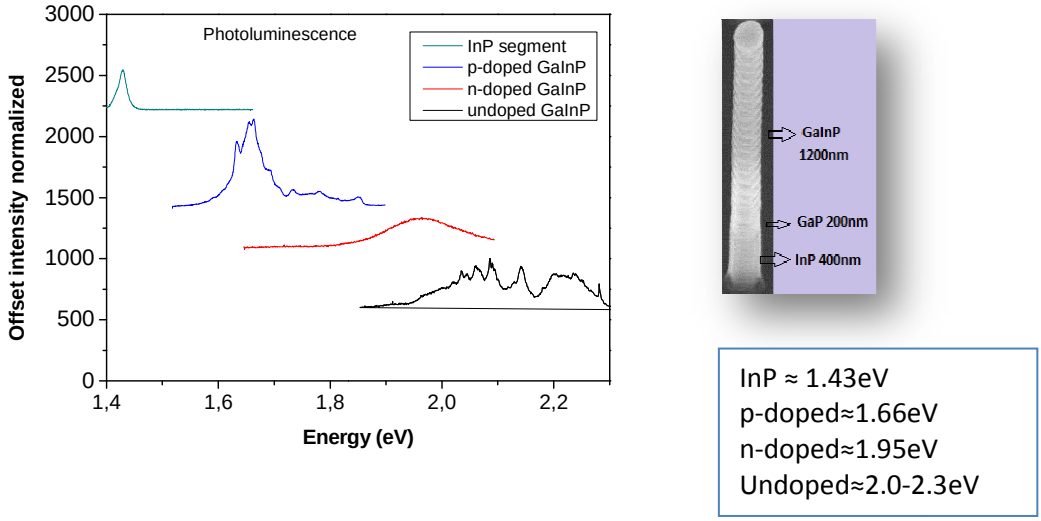

Figure 18: Photoluminescence spectra obtained at low temperature (5-10K) for 3 different single NWs (p-doped, n-doped and un-doped) both with a bottom segment of InP (length 400nm) by using a laser at 2.3eV.

By introducing the different precursors, a shift in the band gap is observed which could be related to a change in the composition due to these dopants during the growth. A stronger change is observed for the p-type segment, which could be related to a higher concentration of indium (In) in this region, while the most blue shifted luminescence is the non intentionally doped material.

A peak is observed for all the NWs around 1.43 eV related to the bottom segment around 400nm of InP (InP at room temperature has a band gap around 1.3eV). Looking at the SEM picture it can be distinguished a 200nm segment of GaP but, since it has an indirect band gap, it shouldn´t affect too much to the PL spectrum. The high band gap of GaP material acts as a barrier for the electrons preventing them from diffusing to the low-bandgap InP segment.

4.2 Electrical measurements

4.2.1 n-Contacts

For the n and the p-type NWs, *I-V* curves were obtained to see if the current-voltage dependence shows a linear behavior. For the n-type NWs the source-drain current increases linearly while a source-drain voltage is applied. From the plot, a resistance with one MΩ was calculated. This can be compared with measurements done with n-type InP NWs where the values for the resistances were in the order of tens of kΩ **[6]**. A result for these kinds of

devices linear behavior was obtained but with resistances higher than the last studies with InP NWs. So the contacts done to n-type GaInP NWs seem to be worse but good enough to show linear behavior.

We were unable to know whether the contacts were dominating, and note that the resistance of the complete NW device is around MΩ.

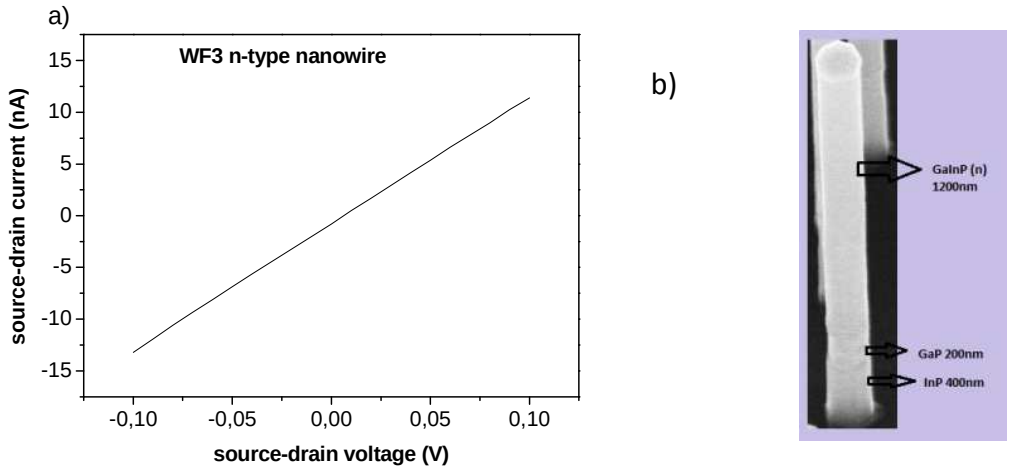

Figure 19: a) Experimental I-V curves from n-doped NWs. b) SEM image of an n-type NW.

Next plots show the behavior of typical n-type contacts where it is possible to see that effectively the application of a positive voltage increases the current, and thus also the conductivity of the device. By sweeping the gate voltage, we can study the doping. These measurements were carried out by applying a sweep back gate voltage.

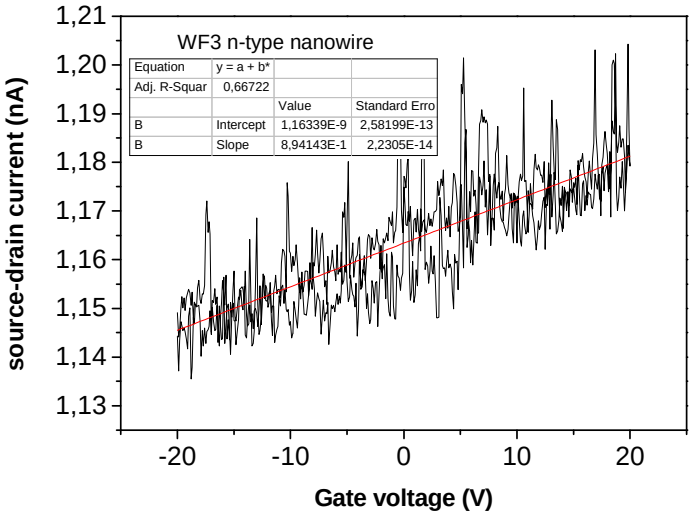

Figure 20: Experimental Gate sweep measurements for n-type contacts, using V_{sd} 0.1V.

The resistivity of the device can be obtained by its relation with the resistance:

$$\rho = \frac{RA}{L} = \frac{R\pi r^2}{L} = \frac{10 \cdot 10^6 \pi (50 \cdot 10^{-9})^2}{1000 \cdot 10^{-9}} = 0.078\Omega m \quad (14)$$

The conductivity was also obtained

$$\sigma = \frac{1}{\rho} = \frac{1}{0.078} = 12.73 Sm^{-1} \quad (15)$$

Note that these measurements were done by working with the total resistance of the device (the sum of the NW and contacts resistance). In order to calculate the electron mobility (μ) , the total capacitance C_{ox} was calculated by the two capacitances of the oxide layers connected in series. The table below summarizes the values for both oxides layers.

	t_{ox} (nm)	ε_r	C_{ox} (F)
SiO_2	100nm	3.7	$1.16 \cdot 10^{-16}$
HfO_2	10nm	25	$2.23 \cdot 10^{-15}$

Table 1: Oxide layer parameters (thickness, relative permittivity and capacitance).

The total capacitance of the two oxides C_{ox} gives a value of $1.102 \cdot 10^{-16}$F. Working with the transconductance from I_d-V_g curve shown in figure 22 gives a value for electron mobility which is unreasonable low:

$$\mu = 5.76 \cdot 10^{-3} \frac{cm^2}{V \cdot s}$$

The low slope obtained for these back gate measurements shows very week gate dependence and may not really reveal the transconductance and thus the mobility. Once the mobility is obtained, Drude model will be useful to calculate the doping concentration but, since a low mobility was obtained, the results will not be reasonable in this case.

4.2.2 p-contacts

Looking at the different plots for the p-type NWs, good electric contacts were not obtained, due to the non linear behavior shown in the plots caused mainly because of Schottky like contacts formed between the metal and semiconductor interface. After all the measurements, it was deduced that making p-type contacts was harder than the n contacts for that kind of NWs where the contacts dominates in p-type case. Comparing again with InP

NWs, the currents in GaInP devices were higher so it means that the contacts designed were a little bit better.

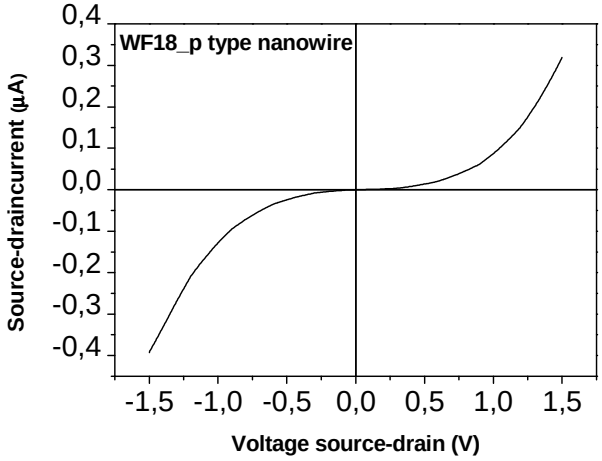

Figure 21: I-V curves measurements for p-doped NWs.

From the gate sweep measurements it can be seen that it is necessary to apply a negative gate bias for an increase in the current. In this case, the devices show p-type behavior but with pretty poor control (showing only a weak dependent effect), which is the case in Schottky curves where the contacts dominate the transport characteristics.

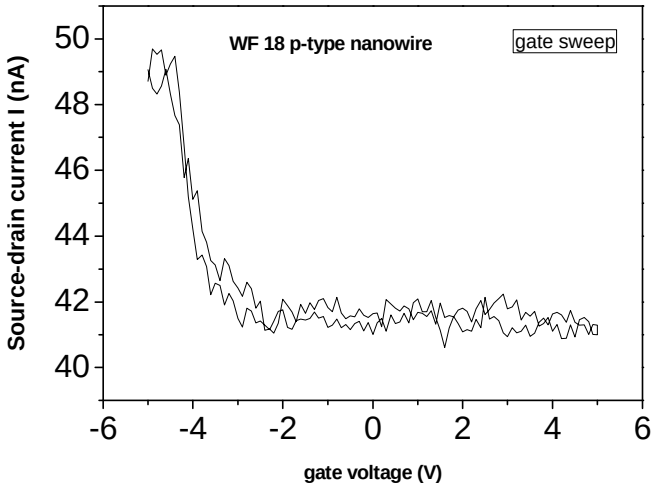

Figure 22: Gate sweep measurements for p-type contacts

As the contacts were highly resistive, the conductivity and mobility are no longer defined by the NW but rather by the contacts. Both n and p-type gate sweep measurements present hysteresis which is probably originated from water dipoles or native oxides which involve screening effects.

4.2.3 p-i-n junction devices in dark

Once n and p-type contacts where designed, p-i-n junction and tunnel diodes have been studied for their application in solar cells.

Electrical measurements were taken for p-i-n junction samples, where only current in the forward direction was seen, which is the behavior expected. Laser excitation (a pointing laser of $\sim$ 2.3eV) was also used to see if photocurrent was generated. Most of the devices showed the characteristic curve under light, but other devices didn´t respond to light excitation. All the p-i-n junctions were fabricated basically under the same conditions except for the etching step where few changes were done. The next table summarizes the p-i-n junction samples.

Sample name	Chemical	Processing time
Laurab7	HF	1min
Laurab8	HF	1min
Laurab10	H_3PO_4 :H_2O /H_2SO_4	2min/1min
Laurab11	HF	25s

Table 2: p-i-n junctions under different etching and passivation conditions

The point of this variation in the etching step was done concerning to the leakage problems observed during the back gate measurements. As it was said before, the conditions of etching and passivation were changed by using HF for 25s instead of 1min (as for samples laurab7,8,9), This was done to see if better condition of the back gate measurements was achieved which shows leakage problems maybe because of some holes in the oxide due to the HF. However, studies have been executed about the rate etching of HF in HfO_2 which etches 1-2nm of HfO_2 per minute and the oxide layer of HfO_2 used for these devices was about 10nm. But after the measurements, still leakage problems appeared (not showed in these plots) where the source-drain current was the same as the gate current which was supposed to be smaller. This characteristic is not important for photocurrent measurements, so no more samples were fabricated at this point.

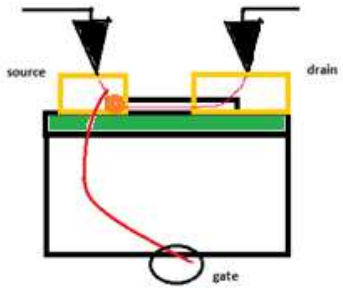

Figure 23: Schematics of how the sample is probed, red lines show I_{sd} and I_{gate} currents.

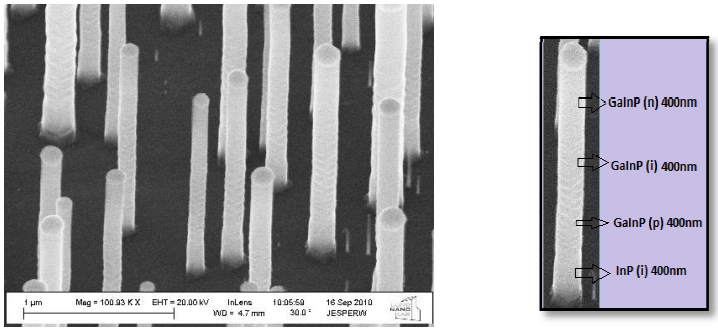

Figure 24: SEM images of a p-i-n junction NW showing the different regions.

Results from the measurements of these devices are shown in the next plots where current is seen only in the forward bias, obtaining the rectifying behavior.

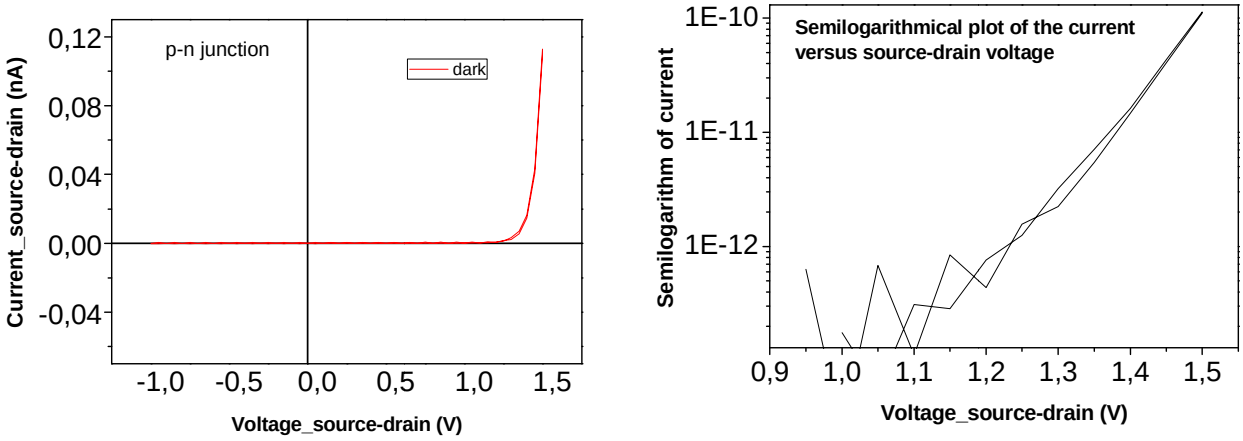

Figure 25: a) I-V curve of p-i-n junction NW (dark current measurements), b) Semilogarithmic plot of I_{sd} versus V_{sd} bias

For these devices, onset values were obtained at 1.2-1.3 V and currents of 10-50nA at 1.9V. The onset value is related to the difference between the Fermi levels in the p and n-type regions; it gives an idea about the band gap of the material. In these measurements the value obtained is lower than the band gap measured from photoluminescence (chapter 4.2.1), which is expected. From the linear region of the *ln(I)-V* characteristics, the ideality factor was calculated.

	ideality factor (n)
Laurab10	2.6
Laurab11	2.1-2.3

Table 3: ideality factor (n) values for the p-i-n junctions

The ideality factor seems to be a little bit larger than 2, which could be related with the non-linear p-contact which increases this parameter. This indicates also that some recombination occurs in the depletion region, and it has been studied with electroluminescence measurements that will be shown in chapter 4.3.1.

4.2.4 p-i-n junction devices under illumination

A pointing laser at 2.3eV was used in order to excite the device. Both dark and light curves are plotted together to see the relation under illumination.

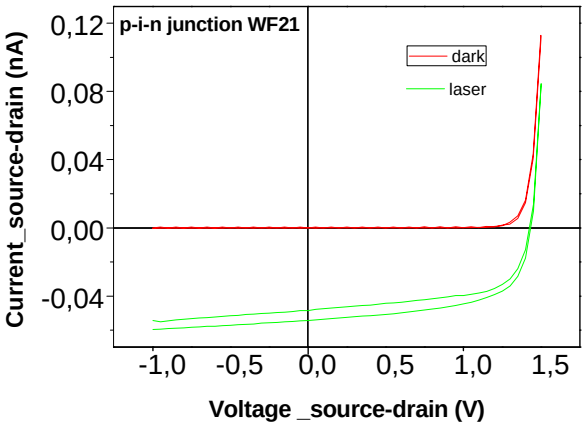

Figure 26: I-V curve of p-i-n junction NWs under illumination with a pointing laser (laurab11).

As mentioned before, some of the most important parameters of p-n junctions focus on solar cells are I_{sc}, V_{oc} and the filling factor. The table below summarizes the values obtained for these p-i-n junctions:

	$I_{sc}\,10^{-12}(\mathrm{A})$	$V_{oc}\,(\mathrm{V})$
Laurab10	10-20	1.35-1.40
Laurab11	10-60	1.35-1.40

Table 4: Isc, Voc values for the p-i-n junctions

Short-circuit current was obtained under illumination with a pointing laser which predicts no too much photocurrent due to the low intensity of it. Hence, the values obtained were around pA. At the same time, the open circuit voltage for these devices was 1.35-1.40V. The filling factor was calculated in the range of 0.5-0.7.

4.3 Optical measurements

Different optical measurements were done in order to study the reaction of our devices under illumination with light, which give us information about the absorption and emission processes. One of the most important parameters we have been focused on is the band gap of these GaInP NWs which is suitable for working on the higher region segment of the Tandem Solar cell objective.

4.3.1 Electroluminescence

Electroluminescence is defined as the light emission of a material in response to an electric current through the material. In semiconductor materials in general and p-n junctions in particular, electroluminescence can be observed due to emission of photons when electrons in the conduction band recombine with holes in the valence band releasing an excess energy corresponding approximately to the band gap.

Electroluminescence characterization was performed by using a camera and a computer program, and by applying a positive bias of around 2.4-2.7 V to the NW device, which leads to a current flowing through the device.

a) 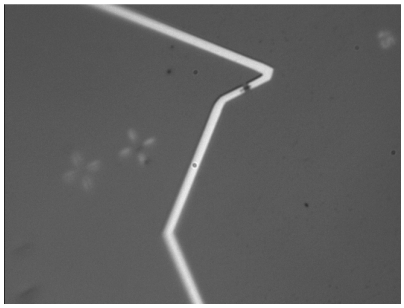 b) 

Figure 27: a) Image taken with a CCD of one device under LED illumination ;b) (EL) image on the CCD from the same device in the dark, at 2.7V for 0.5s of integration time.

In order to study the recombination processes over the band gap of the material, we first tried to evaluate the wavelength of the emitted light by using different filters (500nm, 550nm, 650nm and 700nm). The filters used were longpass (LP) filters which are colored glass filters that attenuate shorter wavelengths and transmit longer wavelengths over the active range of the target spectrum (ultraviolet, visible, or infrared).As revealed by the different CCD images, some light could be observed coming from the device independently of the filter. Unfortunately this crude method could not be used to estimate the emission wavelength.

In order to investigate the electroluminescence further, a spectrum was taken while a certain voltage of 2.3V was applied across the device at room temperature.

a) 

b) 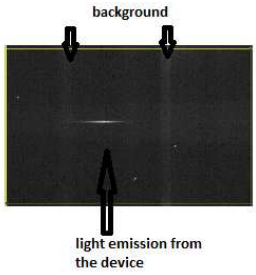

Figure 28: a) Device selected for electroluminescence measurements from microscope lamp. b) Electroluminescence detected from the device at 2.3V bias via difracttion grating.

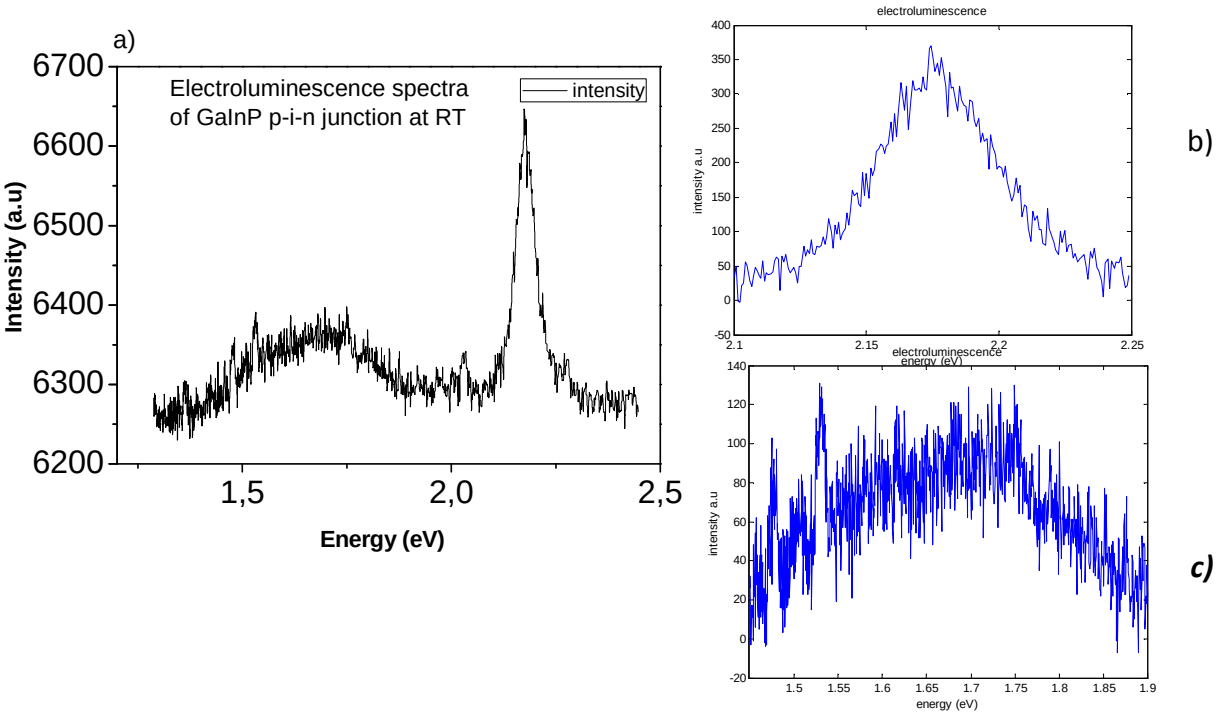

Figure 29: a) Electroluminescence spectrum taken at room temperature on a single device

with 2.3V applied bias; integration time of 1min. b) Normalized peak (2.1-2.3eV) from spectra in Figure 42 a); c) Normalized peak(1.4-1.85eV) from spectra in Figure42a).

The room temperature electroluminescence spectra reveal two peaks, a sharp peak around 2.17eV (in the yellow region) corresponding to the band gap of the un-doped region observed by PL (which was done at low temperature). In addition, we observe a broader peak around 1.68eV, which is close to the PL emission energy observed when measuring p-type GaInP NWs of 1.66 eV, and could be related to band to band electron-hole pair recombination of free carriers in the p-region. This peak could be also influenced by the n region at 1.8eV which appeared at 1.95eV at low temperature for the PL measurements. The full width at half maximum value of the peaks was 61meV for the sharp peak and 300meV for the broader peak. As a comparison, electroluminescence measurements have previously been reported from InP NWs under a 1.6V bias, showing a peak centered at 1.33eV with a full width at half maximum value of 100meV **[27]**.

It is known that the thermal energy at room temperature can ionize donors and acceptors so in contrast with PL measurements that were taken at low temperature, the electroluminescence spectrum should show broader peaks with lower intensity, while for lower temperatures sharper peaks should appear. But this is not what the measurements reveal, where a sharper peak is observed in the un-doped segment for EL measurements. In electroluminescence, the measurements obtained are related to the emission of photons due to recombination of electrons in the depletion region, but in photoluminescence, the emission comes from all over the sample which could vary along the wire obtaining a broader peak than what we expected. However, the energy of the two peaks from EL is very similar to that of the PL ones.

Electroluminescence was done focused onto individual NWs by means of a microscope objective ($\times 50, numerical\ aperture\ NA = 0.5$). The emitted EL intensity is proportional to the current density through the device. The quantum efficiency (QE) of the device is about $4 \cdot 10^{-8}$at room temperature, assuming a 2% detection efficiency in our setup. The detection efficiency of the set up was obtained by taking into account several losses due to lenses, mirrors, grating and also the numerical aperture of the optical microscope.

$$QE = \frac{output}{input} = \frac{photons/s}{current} = \frac{photons/s}{electrons/s} = \frac{16308}{6.5 \cdot 10^{-9}} = 4 \cdot 10^{-8} \quad (16)$$

The emission intensity as function of the current through the device has been studied previously in InP NWs with a quantum efficiency around $1 \cdot 10^{-5}$at room temperature with a 10% detection efficiency of the set up used **[27]**. Even though our efficiency detected in our set-up was lower (2%) compared with the InP measurements, the quantum efficiency obtained was really small. One reason for that could be some losses due to non-radiative recombination, because of a change in the band structure related with a change in composition during the doping. This could also be because of non-optimized device processing.

The broader peak gives us 58105.83 photons/s (with a QE ≈ $1.43 \cdot 10^{-7}$), which gives information about the electron-hole recombination that takes part in the NW, which apparently is more predominant in the p-region which has a lower band gap than the un-doped and n-doped region.

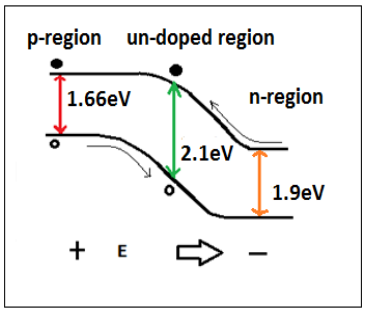

Figure 30: Schematic of the band diagram showing recombination that might take place in the device.

Figure 30 shows the behavior of the band diagram for these p-i-n junctions under a specific bias applied, which makes the electrons to move in the opposite direction of the electric field and recombining on its way mostly in the un-doped region (band gap of 2.1eV) and in the p-region (with a lower band gap ≈1.67eV).

4.3.2 Photocurrent dependence on laser intensity

After EL characterization, photocurrent measurements were done by illuminating with a green laser for different intensities in order to try to understand the low EL efficiency.

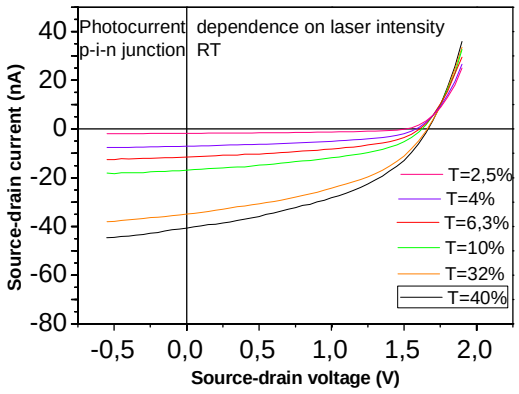

Figure 31: Photocurrent dependence on the laser intensity (P=0.042W). T is the transmission of the laser power through the filters.

Looking at the plot in Figure 31, it is possible to see how the photocurrent generated due to the illumination of the device with a green laser focused onto an individual NW by the microscope objective, is increased when the intensity of the laser is higher. The control of this power is done by using different filters that transmit a percentage of the intensity of the laser.

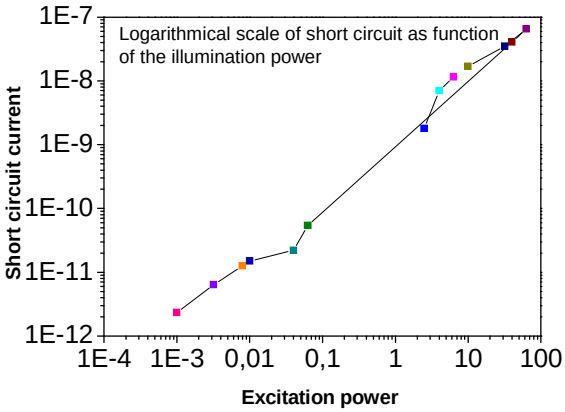

Figure 32: Short circuit current (I_{sc}) dependence of the laser intensity

From Figure 32, a linear fit of the ln*(I_{sc})* versus ln*(P)* was made, calculating the slope of 0.969. An almost linear behavior of the increase of the photocurrent due to the increase of the intensity of the laser is observed.

$$I_{sc} = p^a \rightarrow \ln(I_{sc}) = a \cdot \ln(p) \rightarrow a = 0.969$$

This was expected because the more focus the laser is on the device, more light will arrive at the junction involving more carriers.

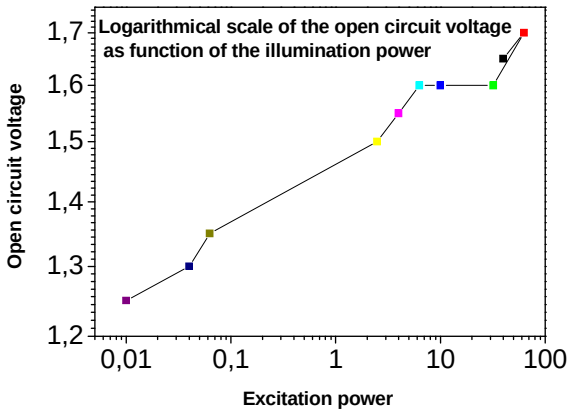

Figure 33: Open circuit voltage (V_{oc}) dependence of the laser intensity

The open circuit voltage varies with the intensity of the laser since it depends on the light generated current (see equation 9). A fit was performed from the V_{oc} versus ln*(p)* obtaining a slope of 0.049 which is two times the thermal energy $\frac{kT}{q} = 0.0258\ (RT)$.

$$slope = \frac{nkT}{q} = 0.049$$

4.3.3 Photocurrent spectroscopy

As it was shown in chapter 4.2.4, by illuminating the p-i-n junction devices with a pointing laser, a response in photocurrent was observed. The pointing laser was a green laser, the value of the band gap wasn´t possible to be calculated. However, what we knew is that the photons that arrive at the device and absorbed, had higher energy than the band gap. So what we have observed at the moment is the response of these devices under illumination with light.

With the intention of getting a more accurate value for the band gap of these NWs, photocurrent spectroscopy was done with a Supercontinuum Source SC450. A regular laser (in the infrared) operates with short laser pulses. Due to the high power amplifier and the high nonlinearity optical fiber, the pulses experience large spectral broadening covering the spectrum from below 450nm to greater than 1750nm. For these measurements, a sweep was done in the range of 500-650nm using a spectrometer.

A chopper was used to eliminate the noise and the background and obtain a smooth signal, the integration time was 1s, with 200Hz, slit of 0.2mm and sensitivity of 100nA/V.

a) 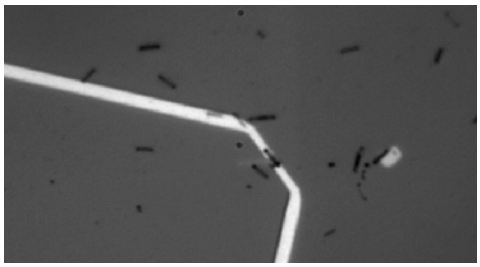 b) 

Figure 34: a) Device selected for photocurrent spectroscopy measurements. b) Laser illuminating the NW.

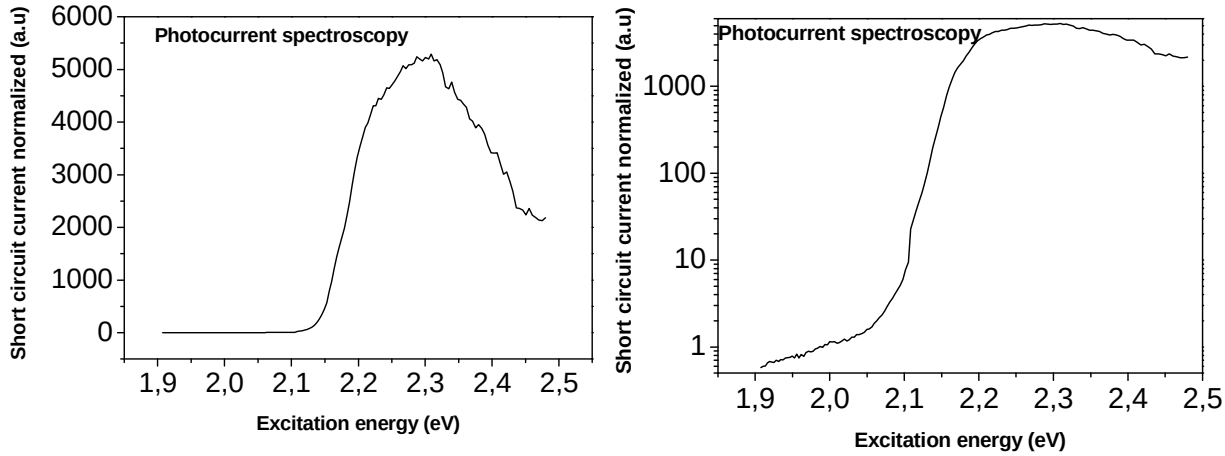

Figure 35: Response of the p-i-n junction GaInP NW due to the different excitation wavelengths. a) Normalized photocurrent as function of the energy. b) Semi logarithm of the normalized current versus energy.

Due to the power dependence of the light source with the different wavelengths, the curve was normalized. It is possible to see how the response of the device as a result of the incoming light, is decreased when the energy of the photons is lower than the band gap

which is around 570-580nm (2.13-2.17eV). So the absorption of these GaInP NWs is in the yellow-green region.

It is also possible to appreciate a non expected behavior around 2.3-2.45eV (500-540nm) where the photocurrent generated decrease for higher energies. This could be related to the power variation of the light source with the change in energies but also because of the coupling of the light into the wire. In addition, the absorption characteristics of the NWs are mainly influenced by their structure.

4.4 Tunnel diodes

Even though the goal of the project was the study of p-i-n junctions for solar cell applications, as we have said in the introduction, the segment heterojunctions of the tandem solar cell example are connected via esaki diodes. We haven´t gone into detail with these devices that are difficult to interpret due to their complexity. Only two tunnel diode devices were fabricated and studied.

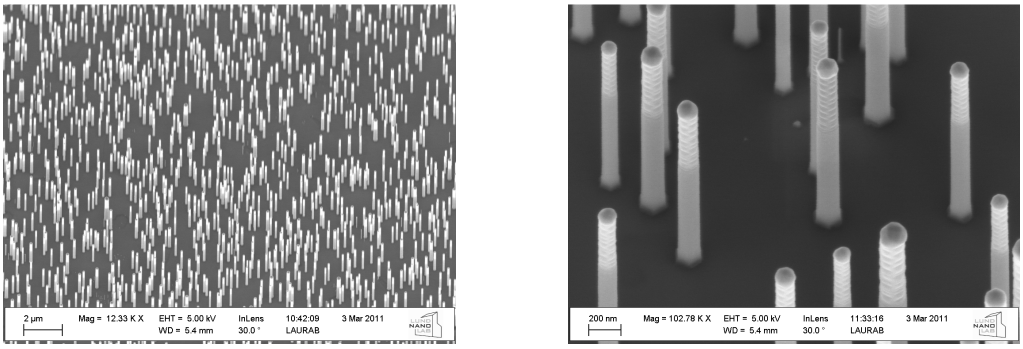

Figure 36: SEM images of Tunnel diode (InP (n^-)-GaInP(p^+)) after being synthesized by MOVPE technique.

Two samples of pure tunnel diodes InP(n^-)-GaInP (p^+) were characterized by measuring *I-V* curves. Both samples were made under the same steps of EBL, etching and passivation, except for the evaporation step, where the deposition of the metal contacts varied. For the first sample, Laurab12 , n-type contacts were designed in both extremes of the NWs by depositing different thickness of metals (Ti/Pd/Au) giving an n-type behavior. For Laurab13 other metals were deposited (Pd/Zn/Pd/Au). So by introducing Zn, p-type contacts were obtained. The liftoff process was successful in both cases. The electrical measurements were carried out at room temperature.

Trying to obtain the typical behavior of tunnel diodes, the measurements have been focused around (-0.3-0.3) V. Looking at the graphics below, it is easy to appreciate very poor tunnel diodes without a specific negative differential resistance (NDR) region which indicates weak band-to-band tunneling. The electron transport in these tunnel diodes is not solved. Different curves were obtained as linear, symmetric or asymmetric and rectifying, where, current in both directions is observed.

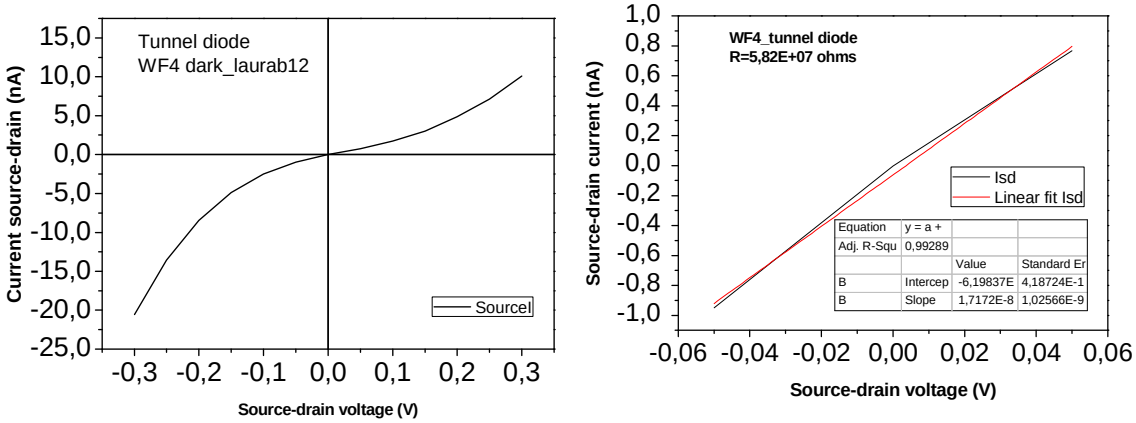

Figure 37: a) I-V curve of the attempted tunnel diode device.b) Figure 38: Linear fit of the I-V curve during the -0.05-0.05V region.

The important parameters for the application of tunnel diodes in solar cells are the peak current density and a very small signal resistance, so a linear fit was done between the region (0.05-0.05) V, where the value of the resistance was calculated by the simple application of Ohm´s law.

The resistance obtained varied along the different devices with values between 50-500MΩ. In reference with tunnel diodes of InP/GaAs, 50MΩ of small-signal resistance was achieved **[6]**.

It´s also useful to study the breakdown voltage in the reverse bias, if the semiconductor is heavily doped, by applying a few volts we will obtain current due to tunneling. For avalanche case (which is also a type of breakdown voltage) several volts must be applied, around 20 V. The avalanche case, is observed when we don´t have a high doping.

In these devices (Laurab13) 5V was applied but the breakdown voltage was not seen. Probably the junctions are not sufficiently doped, but we note that poor contacts may dominate the I-V characteristics, shadowing any tunneling. There is a possibility of getting a

good contact in the n region (that what we get before when we were working with the n-contacts), while a bad contact in the p side could be present which produce a higher barrier that makes it difficult for the transport of the electron showing the rectifying characteristics. This seems to be quite congruent due to latest results about contacting n and p sides where p sides were more difficult to contact.

As it has been shown, contacting and interpreting Esaki tunnel diodes is not trivial and more investigation must be done in this area.

5. CONCLUSIONS

In order to contribute to AMON-RA project, which is focused on the fabrication of an inexpensive and high efficiency tandem solar cell based on p-n junction NWs, the aim of this project was the study of GaInP NWs expected to be used on the top cell of a multijunction tandem solar cell. Field effect transistors (FETs) NWs were fabricated and characterized by optical and electrical means. To be able to work with these p-i-n junction devices, first, p and n-type contacts were studied by applying a back-gate bias through the device, providing a p and n-type behavior. NWs with p-i-n doping show excellent rectification with reasonably low ideality factors. Moreover, these p-i-n junctions were measured by illumination with a pointing laser showing a short circuit current $\sim 40\mathrm{pA}$, with an open circuit voltage of 1.35-1.40V,which was expected to be lower than the band gap obtained in photoluminescence (at low temperature) measurements for the un-doped region at 2.17 eV.

In addition, photoluminescence measurements on three different single NWs of GaInP grown with specific precursors (giving a p, n and un-doped regions) were studied at low temperature on an Au substrate. The spectra show three emissions at different energy related to the three types of NWs. This shift in energy could be related to the change in composition during the growth due to the addition of diverse precursors (Hydrogen sulfide (H_2S) as n-type doping precursor and diethyl zinc (DEZn) as a p-dopant precursor). Transmission electron microscopy (TEM) images for these NWs might have helped us giving important information to try to understand what is going on when these NWs are doped

with different precursors, in the same as energy dispersive X-ray spectroscopy (EDX) measurements which are used to analyze the chemical composition of the NWs.

In order to study in more detail the band gap of the material, electroluminescence spectra was taken at room temperature showing two predominant peaks at 1.68eV and 2.174eV which were connected to the PL(at low temperature) results for the p and un-doped NWs, at 1.66 and 2.1-2.3 eV respectively. The low quantum efficiency measured was mainly related to the relative low current through the not optimized device, possibly escape of the carriers from the depletion region, and also some non-radiative recombination as a result of the possible change in the band structure along the wire. In order to avoid thermal excitation of the electron to higher levels, future optical measurements at low temperature will be useful for accurate results.

Photocurrent dependence on the laser intensity was also measured, were important parameters for solar cells, (V_{oc} and I_{sc}) vary as function of the power of the light incoming through the device. Future measurements of photocurrent at low temperature could give information about how these parameters change due to the change in temperature.

Photocurrent spectroscopy was done on p-i-n junction NWs by illuminating the device at different wavelengths near the band gap region in order to see the decrease of the light generated current while the energy of the incoming photons was approaching to the limit ($hv < E_G$).

Coming back to the AMON-RA project, GaInP NWs seem to be a promising material to be used in the top cell of this tandem junction solar cell.

6. ACKNOWLEDGEMENTS

First of all I will like to give a special thanks to my supervisors Jesper Wallentin and Magnus Borgström for accepting me working on this fascinating project and for the nice treatment all over this year, for their assistance and for solving all my questions. I also appreciate all the help from Dan Hessman with the photocurrent spectroscopy measurements and my

colleague Anna Jansson for her involvement in this project. Also to Kilian Mergenthaler related to the photoluminescence measurements. Thanks to all the nanolab personnel that have helped me inside the lab, especially Ivan Maximov, and all the people from Solid State division for always being there for listening and helping. I will like to mention my gratitude to Knut Deppert and Lars Samuelson for giving me the opportunity of making my master thesis project in this nice division of Lund University.

7. REFERENCES

[1] O. Schultz, R. P. S. W. G., Fraunhofer ISE, Freiburg, Germany ; A. Mette, Q-Cells AG, Thalheim, Germany, Silicon Solar Cells with Screen-Printed Front Side Metallization Exceeding 19% Efficiency. In *22nd European Photovoltaic Solar Energy Conference and Exhibition*, Milano, Italy, **2007**.

[2] http://www.pveducation.org/pvcdrom/solar-cell-operation/solar-cell-structure

[3] Dimroth,F and Kurtz,S. "High-efficiency multijunction solar cells," MRs Bull., vol.32,pp.230-235,Mar.**2007**.

[4] Borgström,M.T.; Wallentin,J.; Heurlin,M.; Fält ,S.; Wickert, P.; Leene, J.; Magnusson,M.H.; Deppert,K.; Samuelson ,L. "Nanowires with Promise for Photovoltaics". Ieee Journal of selected topics in quantum electronics.

[5] Hermle.M.; Létay.G.; Philips.P.S.; Bett.A.W. "Numerical Simulation of Tunnel Diodes for Multi-junction Solar Cells". Res.Appl.vol 16.pp 409-418. **2008.**

[6] Wallentin ,J.; Persson , M.; Wganer,J.B.; Samuelson, L.; Deppert, K and Borgström ,M. "High Perfomance Single Nanowire Tunnel Diodes". Nano Lett., vol.10, pp974-979, Mar. **2010.**

[7] Kupec,J and Witzigmann,B. "Dispersion, wave propagation and efficiency analysis of nanowire solar cells,"Opt.Exp.,vol17,pp.10399-10410, Jun. **2009.**

[8] Chan,Y-J.;Pavlidis,D.;Razeghi,M.;Omnes,F. "GaInP/GaAs HEMT's Exhibiting Good Electrical Performance at Cryogenic Temperatures". IEEE Transactions on electron devices. Vol 77, 10, Oct. **1990.**

[9] Khanal D.R., W. J. *Nano Letters***,** 7, (9), pp.2778-2783, **2007**.

[10]http://www.utc.edu

[11] Luque A and Hegedus S, Handbook of Photovoltaic Science and Engineering .Chap 3, The physics of solar cells.Wiley, England, **2003.**

[12] www.solar.udel.edu/ELEG620/05_Illuminatedpnjunctio**n**.pdf

[13] http://www.pveducation.org/solarcells.

[14] S.M. Sze, Semiconductor Devices, Physics and Technology. In John Wiley & Son: **1985**.

[15] Kempa,T.J.; Tian,B.Z.; Kim,D.R.; Hu,J.S.; Zheng,X.L.; Lieber,C.M. "Single and Tandem Axial p-i-n Nanowire Photovoltaic Devices". Nano Letters, vol.8, pp.3456-3460, Oct.**2008**

[16] Shah, J.M.; Li,Y.L.; Gessmann.Th.; Schubert.E.F. "Elemental analysis and theoretical model for anomalously high ideality factors (n≫2.0) in AlGaN/GaN p-n junction diodes". Appl.Physics., vol 94 (4). August **2003.**

[17] Sah,C.; Noyce,R,n, and Shockley.W, Proc. IRE 45, 1228 ,**1957**.

[18] Esaki,L. Phys.Rev.109 (2),603-604, **1958.**

[19] http://www.pfk.ff.vu.lt.vu.lt/lectures/funkc_dariniai/diod/p-n_devices.htm

[20] Ivey D,G. "Platinum Metals in Ohmic Contacts to III-V Semiconductors". Platinum Metals Rev., vol 43, (1), pp.2-12, **1999.**

[21] *http://www.eecs.umich.edu/~singh/bk7ch07.pdf*

[22] Zhang Z.; Yao K.; Liu Y.; Jin C.; Liang X., Chen Q, and Peng L.M. "Quantitative analysis of current voltage characteristics of semiconducting nanowires : Decoupling od contacts effects". *Advanced functional materials, 17, pp.2478-2489,**2007.***

[23] http://fillergroup.gatech.edu/research/

[24] E.I. Givargizov, J.Cryst.Growth,31,p.20, **1975**.

[25] Borgström M,T.;, Wallentin J.; Trägardh J.; Ramvall P.; Ek M.; Wallenberg L.R.; Sameulson L, and Deppert K. "In situ Etching for Total control over Axial and Radial Nanowire Growth". Nano Res, 3:264-270, **2010**.

[26] http://nanodim.kristianstorm.com

[27] Borgström M.T.; Norberg E.; Wickert P.; Nilsson H.A.; Trägardh J.; Dick K.A.; Statkute G.; Ramvall.P.; Deppert.K and Samuelson.L. "Precursor evaluation for in situ InP nanowire doping". Nanotechnology, 19, 445602, **2008**.